SSCL-N-863

SSCL-N-863
May 1994
Distribution Category: 400

G. Dugan

Hydrogen Density Distribution Analysis in SSC Beam Pipe Materials and Connection to Photodesorption Coefficients in a Diffusion Model

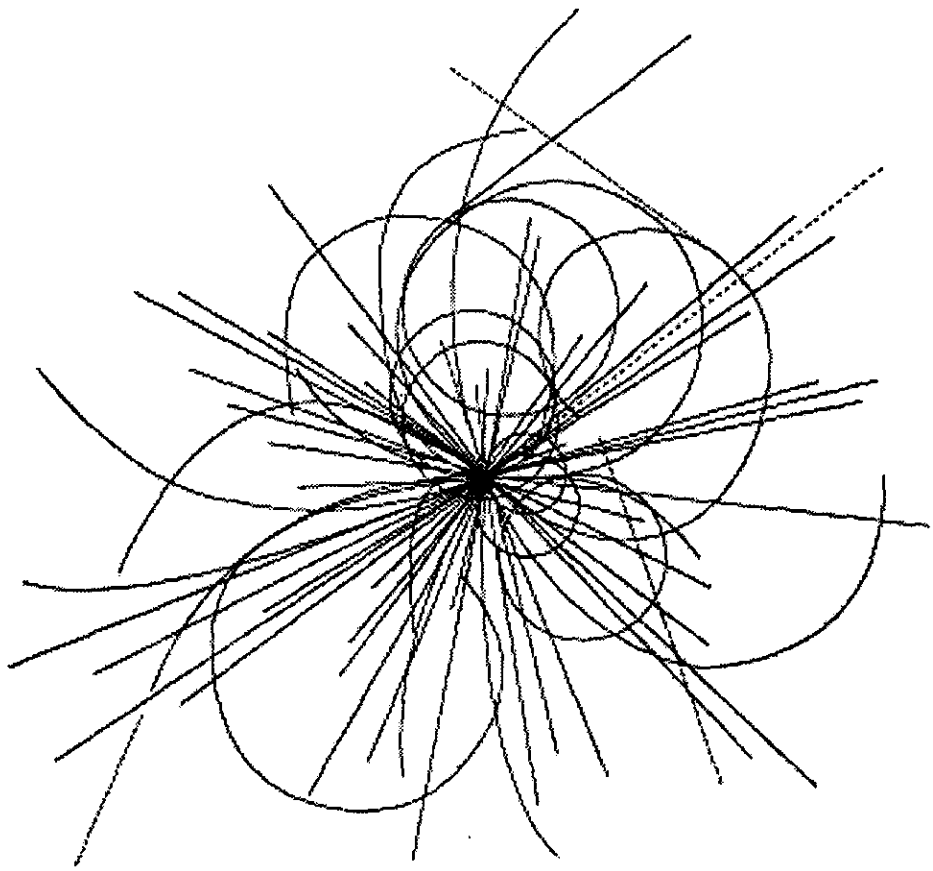

Superconducting Super Collider Laboratory

SSCL-N-863

Hydrogen Density Distribution Analysis in SSC Beam Pipe Materials and Connection to Photodesorption Coefficients in a Diffusion Model

G. Dugan

Superconducting Super Collider Laboratory*
2550 Beckleymeade Ave.
Dallas, TX 75237, USA

May 1994

*Operated by the Universities Research Association, Inc., for the U.S. Department of Energy under Contract No. DE-AC35-89ER40486.

1.0 Introduction

Recent measurements[1] utilizing a technique[7] based on nuclear reactions of heavy ions bombarding metals have allowed the measurement of the concentration density of hydrogen atoms chemically bound within these metals. By assuming a simple diffusion process[2] to account for the transport of hydrogen from the interior of the metal to the surface, this information can be related to the process of photodesorption, wherein hydrogen is evolved from the surface of a metal through bombardment by UV photons.

The diffusion model described in Ref. 2 relates the photodesorption coefficient to the hydrogen concentration density for some particular analytic forms of the density distribution. In this paper, the model is expanded to cover more general forms of the concentration density, such as have been reported in Ref. 1. The data in Ref. 1 is analyzed to extract density distributions for the atomic hydrogen chemically bound in metal samples. These empirical density distributions are then used in the diffusion model equations to obtain predictions for the photodesorption coefficient. The predictions, which contain several unknown parameters, are then compared with experimental photodesorption coefficient data, to extract values for the unknown parameters.

2.0 Development of the Relation Between the Photodesorption Coefficient and the Hydrogen Density Distribution in a Diffusion Model

In Ref. 2, the background for the development of the parameters, constants, and equations involved in the diffusion model is presented. One of the two fundamental parameters is the following:

$$\kappa = \lambda \sigma_D(E,M). \tag{1}$$

In this equation, λ represents the mean depth within the metal over which the photons interact with the hydrogen atoms to produce atoms which emerge from the surface, and $\sigma_D(E,M)$ is the cross section for the fundamental photodesorption process. The other fundamental parameter is D, the diffusion constant for hydrogen atoms within the metal.

As in Ref. 2, we assume here that, either as a result of photon scattering, or through the process of photoelectron production followed by subsequent electrodesorption, the entire tube circumference is involved uniformly in the desorption process. The (uniform) photon flux incident on the surface is designated by $\dot{\gamma}$.

If we let c(x,t) be the volume concentration of gas *molecules* at a distance x from the surface within the metal at time t, then the molecular flux evolved by the photodesorption process, $\Phi(t)$, is

$$\Phi(t) = \kappa\, c(0,t)\dot{\gamma} \tag{2}$$

and the photodesorption coefficient (in molecules/photon) is

$$\eta = \Phi / \dot{\gamma}. \tag{3}$$

In the diffusion model, the molecular concentration density c(x,t) satisfies the diffusion equation,

$$D\frac{\partial^2 c(x,t)}{\partial x^2} = \frac{\partial c(x,t)}{\partial t}, \tag{4}$$

subject to the boundary condition

$$\Phi(t) = D\frac{\partial c(0,t)}{\partial x} = \kappa\, c(0,t)\dot{\gamma} \tag{5}$$

and an initial condition determined by the initial concentration density c(x,0).

In Ref. 2, solutions are developed to these equations for two specific functional forms of the initial concentration density, c(x,0). However, it is possible to solve Eqs. (4) and (5) for a general initial concentration density, provided only that c(x,0) is constant or decreasing as $x \rightarrow$ infinity. The technique is the same as outlined in Ref. 2, *i.e.*, the method of LaPlace transforms. The general result is

$$c(x,t) = \int_x^\infty \left\{ \frac{\mathrm{Exp}[\frac{-u^2}{4Dt}]}{2\sqrt{\pi Dt}} - \frac{k}{D}\mathrm{Exp}\left[\frac{k(kt+u)}{D}\right]\mathrm{Erfc}\left[k\sqrt{\frac{t}{D}} + \frac{u}{2\sqrt{Dt}}\right] \right\} c(u-x,0)du$$
$$+ \int_{-x}^\infty \frac{\mathrm{Exp}[\frac{-u^2}{4Dt}]}{2\sqrt{\pi Dt}}\, c(u+x,0)du \qquad (6)$$

in which $k = \kappa\dot{\gamma}$. This gives for $\eta(t) = \kappa\, c(0,t)$,

$$\eta(t) = \kappa \int_0^\infty \left\{ \frac{\mathrm{Exp}[\frac{-u^2}{4Dt}]}{\sqrt{\pi Dt}} - \frac{k}{D}\mathrm{Exp}\left[\frac{k(kt+u)}{D}\right]\mathrm{Erfc}\left[k\sqrt{\frac{t}{D}} + \frac{u}{2\sqrt{Dt}}\right] \right\} c(u,0)du\,. \qquad (7)$$

As will be discussed below, the experimental data from Ref. 1 for the *atomic* hydrogen concentration density, $c_A(x)$, can be well fitted to a sum of three exponentials:

$$c_A(x) = \sum_{i=1}^{3} c_i \mathrm{Exp}(-x\Lambda_i)\,. \qquad (8)$$

If we assume that the initial molecular concentration density is related to the atomic concentration density by

$$c(x,0) = c_A(x)/2\,, \qquad (9)$$

then Eqs. (7) to (9) give

$$\frac{\eta(t)}{\kappa} = \sum_{i=1}^{3} \frac{c_i}{2}\left[\frac{\mathrm{Exp}(\frac{t}{\tau})\mathrm{Erfc}[\sqrt{\frac{t}{\tau}}] - \mathrm{Exp}(\frac{t}{\tau_{p_i}})\sqrt{\frac{\tau}{\tau_{p_i}}}\,\mathrm{Erfc}[\sqrt{\frac{t}{\tau_{p_i}}}]}{(1 - \sqrt{\frac{\tau}{\tau_{p_i}}})} \right]\,, \qquad (10)$$

where

$$\tau = \frac{D}{(\kappa\dot{\gamma})^2} \quad \text{and} \quad \tau_{p_i} = \frac{1}{\Lambda_i^2 D}\,. \qquad (11)$$

3.0 Analysis of Nuclear Reaction Data to Derive Atomic Hydrogen Density Distributions

The atomic hydrogen concentration in the metal, $c_A(x)$, was measured in Ref. 1 by bombarding a sample of the metal with a monoenergetic beam of $E_0 \cong 6.4$ MeV ^{15}N ions. The ^{15}N ions penetrate into the metal and lose energy primarily due to inelastic collisions with the atomic electrons at a (constant) rate which we call dE/dx. The energy of the beam at a distance x within the metal is thus given by

$$E(x) = E_0 - (dE/dx)x. \tag{12}$$

The ^{15}N ions undergo nuclear reactions with the nuclei of the metal atoms, and also with the protons associated with hydrogen atoms embedded within the metal. The nuclear reaction with hydrogen,

$$^{15}N + H \rightarrow {}^{16}O \rightarrow {}^{12}C + {}^{4}He + \gamma.$$

has a strong, narrow resonance at $E_r = 6.385$ MeV, with a resonance width of $\Gamma = 1.8$ keV. The energy dependence of the cross section is taken as that of the standard Breit-Wigner form,

$$\sigma(E) = \frac{\sigma_0 \frac{\Gamma^2}{4}}{\frac{\Gamma^2}{4} + (E-E_r)^2}, \tag{13}$$

where σ_0 is the cross-section on resonance.

When the ^{15}N ions have penetrated a distance x such that $E(x) = E_r$, the above nuclear reaction results in the production of gamma rays, which have an energy of about 4.43 MeV. The total number of gamma rays, N_γ, produced by an ion beam of N ions of initial energy E_0 is

$$N_\gamma = N \int_0^\infty c_A(x)\, \sigma(E(x))\, dx, \tag{14}$$

where E(x) is given by Eq. (12). By measuring the number of gamma rays as a function of the ion beam energy E_0, the density distribution $c_A(x)$ within the metal can be mapped out.

The spatial resolution of this method depends in principle on the resonance width Γ, as can be seen by combining Eqs. (13) and (14). In addition, there are other important effects[7]. The dominant contributors are the finite spread in energy in the initial ion beam (σ_b), the energy spread of the ions due to straggling as the beam loses energy in the metal (σ_S), and the relative ion-atom energy spread due to vibrational motion of the hydrogen atoms in the metal lattice (Doppler broadening, σ_D) . These three effects can be well approximated by assuming a Gaussian distribution for the energy of the ions:

$$\frac{dN}{dE} = \frac{N}{\sqrt{2\pi}\sigma_E} Exp\left[\frac{(E-E(x))^2}{2\sigma_E^2}\right] \tag{15}$$

where $\sigma_E^2 = \sigma_D^2 + \sigma_S^2 + \sigma_b^2$. The square of the energy spread due to straggling, σ_S^2, is a linear function of the depth of penetration of the ion beam, x: $\sigma_S^2 = k_S x$, where k_S is a calculable constant. Substituting Eqs. (12), (13) and (15) into (14), we have

$$N_\gamma = N \frac{\sigma_0 \frac{\Gamma^2}{4}}{\sqrt{2\pi}\sigma_E} \int_0^\infty c_A(x)dx \int_{-\infty}^{\infty} \frac{\mathrm{Exp}\left[\frac{\left(E'-E_0+\frac{dE}{dx}x\right)^2}{2\sigma_E^2}\right]}{\frac{\Gamma^2}{4}+(E'-E_r)^2} dE' . \quad (16)$$

The energy integral can be done exactly, using[3]

$$\int_{-\infty}^{\infty} \frac{y\,\mathrm{Exp}(-t^2)}{y^2+(t-x)^2} dt = \pi\,\mathrm{Re}[w(x+I\,y)] , \quad (17)$$

where

$$w(z) = \mathrm{Exp}(-z^2)\,\mathrm{Erfc}(-I\,z) . \quad (18)$$

The result is

$$\frac{\sigma_0 \frac{\Gamma^2}{4}}{\sqrt{2\pi}\sigma_E} \int_{-\infty}^{\infty} \frac{\mathrm{Exp}\left[\frac{\left(E'-E_0+\frac{dE}{dx}x\right)^2}{2\sigma_E^2}\right]}{\frac{\Gamma^2}{4}+(E'-E_r)^2} dE' = \frac{\sigma_{int}}{\sqrt{2\pi}\sigma_E}\mathrm{Re}\left(w\left[\frac{\frac{dE}{dx}x - E_0 + E_r}{\sqrt{2}\sigma_E} + I\frac{\Gamma}{\sqrt{8}\sigma_E}\right]\right), \quad (19)$$

where

$$\sigma_{int} = \int_{-\infty}^{\infty} \sigma(E)dE = \frac{\sigma_0 \Gamma \pi}{2} \quad (20)$$

is the energy-integrated total cross section.

Using Eqs. (19) and (20) in (16) gives the following:

$$N_\gamma = N \frac{\sigma_{int}}{\sqrt{2\pi}\sigma_x \frac{dE}{dx}} \int_0^\infty c_A(x)\mathrm{Re}\left(w\left[\frac{(x-x_0)}{\sqrt{2}\sigma_x} + I\frac{\Gamma_x}{\sqrt{8}\sigma_x}\right]\right)dx , \quad (21)$$

where $\sigma_x = \sigma_E / (dE/dx)$, $x_0 = (E_0 - E_r)/(dE/dx)$, and $\Gamma_x = \Gamma/(dE/dx)$. If we assume the form for the density distribution $c_A(x)$ as given in Eq. (8), then Eq. (21) becomes

$$N_\gamma = N \frac{\sigma_{int}}{\sqrt{2\pi}\sigma_x \frac{dE}{dx}} \sum_{i=1}^{3} c_i \int_0^\infty \mathrm{Exp}(-x\Lambda_i)\mathrm{Re}\left(w\left[\frac{(x-x_0)}{\sqrt{2}\sigma_x} + I\frac{\Gamma_x}{\sqrt{8}\sigma_x}\right]\right)dx \,. \tag{22}$$

The integral in Eq. (22) can be done as follows. Using Eq. (18), that part of the integrand involving the function w(z) can be written as

$$w\left[\frac{(x-x_0)}{\sqrt{2}\sigma_x} + I\frac{\Gamma_x}{\sqrt{8}\sigma_x}\right] = \mathrm{Exp}\left[-\left[\frac{x-x_0}{\sqrt{2}\sigma_x} + I\frac{\Gamma_x}{\sqrt{8}\sigma_x}\right]^2\right]\left[1-\mathrm{Erf}\left[\frac{\Gamma_x}{\sqrt{8}\sigma_x} - I\frac{(x-x_0)}{\sqrt{2}\sigma_x}\right]\right]. \tag{23}$$

This can then be separated into real and imaginary parts using the following equalities:

$$\mathrm{Exp}[-(x + Iy)^2] = \mathrm{Exp}[-x^2 + y^2]\,(\mathrm{Cos}[2xy] - I\mathrm{Sin}[2xy]) \tag{24}$$

and[4]

$$\mathrm{Erf}[x + Iy] = \mathrm{Erf}[x] + \frac{\mathrm{Exp}[-x^2](1 - \mathrm{Cos}[2xy])}{2\pi x} + I\frac{\mathrm{Exp}[-x^2]\mathrm{Sin}[2xy]}{2\pi x} + \frac{2\mathrm{Exp}[-x^2]}{\pi}\sum_{n=1}^{\infty}\frac{\mathrm{Exp}[-\frac{n^2}{4}](f_n(x,y) + Ig_n(x,y))}{n^2 + 4x^2} \tag{25}$$

in which

$$f_n(x,y) = 2x - 2x\mathrm{Cosh}[ny]\mathrm{Cos}[2xy] + n\mathrm{Sinh}[ny]\mathrm{Sin}[2xy] \tag{26}$$

and

$$g_n(x,y) = 2x\mathrm{Cosh}[ny]\mathrm{Sin}[2xy] + n\mathrm{Sinh}[ny]\mathrm{Cos}[2xy] \,. \tag{27}$$

These expressions are inserted into Eq. (23), and the real part is taken as indicated in Eq. (22). The result is a series of integrals of the general form,[5]

$$\int_0^\infty \mathrm{Exp}[-\beta t^2 - \nu t]\mathrm{Cos}[bt]dt = \sqrt{\frac{\pi}{16\beta}}\left\{\mathrm{Exp}[\frac{(\nu - Ib)^2}{4\beta}]\mathrm{Erfc}[\frac{(\nu - Ib)}{2\sqrt{\beta}}] + \mathrm{Exp}[\frac{(\nu + Ib)^2}{4\beta}]\mathrm{Erfc}[\frac{(\nu + Ib)}{2\sqrt{\beta}}]\right\} \tag{28}$$

and

$$\int_0^\infty \mathrm{Exp}[-\beta t^2 - \nu t]\mathrm{Sin}[bt]dt = -I\sqrt{\frac{\pi}{16\beta}}\left\{\mathrm{Exp}[\frac{(\nu - Ib)^2}{4\beta}]\mathrm{Erfc}[\frac{(\nu - Ib)}{2\sqrt{\beta}}] - \mathrm{Exp}[\frac{(\nu + Ib)^2}{4\beta}]\mathrm{Erfc}[\frac{(\nu + Ib)}{2\sqrt{\beta}}]\right\} \tag{29}$$

Use of these formulas then gives an exact result for the integral in Eq. (22). However, the result is complicated in form. As useful simplification results from an expansion to second order in the parameter $\frac{\Gamma_x}{\sqrt{8}\sigma_x}$, appropriate (as in this case) when $\frac{\Gamma_x}{\sqrt{8}\sigma_x} << 1$. The result is

$$N_\gamma = N \frac{\sigma_{int}}{\frac{dE}{dx}} c_{eff}(x_0), \tag{30}$$

where

$$c_{eff}(x_0) = \sum_{i=1}^{3} \frac{c_i}{2} \left[\begin{array}{l} \mathrm{Exp}[\frac{\Lambda_i}{2}(\Lambda_i\sigma_x^2 - 2x_0)](1-\mathrm{Erf}[\frac{\Lambda_i\sigma_x^2 - x_0}{\sqrt{2}\sigma_x}]) \left\{ 1 + \frac{\Gamma_x \Lambda_i^2 \sigma_x}{4\pi\sqrt{2}}(1 - \frac{\Gamma_x \pi}{\sqrt{2}\sigma_x}) + \frac{\Gamma_x}{4\pi\sqrt{2}\sigma_x}(1 - 4\sqrt{\pi}) \right\} \\ - \frac{\Gamma_x(\Lambda_i\sigma_x^2 + x_0)(1 - \frac{\Gamma_x \pi}{\sqrt{2}\sigma_x})}{4\pi^{\frac{3}{2}}\sigma_x^2} \mathrm{Exp}[-\frac{x_0^2}{2\sigma_x^2}] + \frac{\Gamma_x}{\sqrt{2}\pi\sigma_x} \mathrm{Exp}[\frac{\Lambda_i}{2}(\Lambda_i\sigma_x^2 - 2x_0)] \sum_{n=1}^{\infty} h_{n,i}(x_0) \end{array} \right] \tag{31}$$

in which

$$h_{n,i}(x_0) = \frac{1}{n^2}\{\mathrm{Exp}[\frac{\Lambda_i n \sigma_x}{\sqrt{2}}]\mathrm{Erfc}[\frac{\Lambda_i\sigma_x}{\sqrt{2}} - \frac{x_0}{\sqrt{2}\sigma_x} + \frac{n}{2}] + \mathrm{Exp}[-\frac{\Lambda_i n \sigma_x}{\sqrt{2}}]\mathrm{Erfc}[\frac{\Lambda_i\sigma_x}{\sqrt{2}} - \frac{x_0}{\sqrt{2}\sigma_x} - \frac{n}{2}] - 2\,\mathrm{Exp}[-\frac{n^2}{4}](1 - \mathrm{Erf}[\frac{\Lambda_i\sigma_x^2 - x_0}{\sqrt{2}\sigma_x}])\} \tag{32}$$

The terms in the infinite sum over n fall off rapidly as n increases, and the whole sum is multiplied by the small quantity $\frac{\Gamma_x}{\sqrt{8}\sigma_x}$. Hence, an excellent approximation is provided by terminating the sum at n=2.

Data was taken, as explained in Ref. 1, by varying E_0, and hence $x_0 = (E_0 - E_r)/(dE/dx)$, measuring N_γ, and computing $c_{eff}(x_0)$ from Eq. (30). Fitting the result to Eqs. (31-32) above then allows the determination of the unknown parameters of the atomic density distribution (c_i, Λ_i).

In practice, two other quantities in Eqs. (31-32) must also be treated as free parameters in order to obtain good fits to the data. The quantity σ_x is given by

$$\sigma_x^2 = (\sigma_D^2 + \sigma_b^2 + k_S x_0)/(dE/dx)^2 = \sigma_{x0}^2 + k_S x_0/(dE/dx)^2 . \tag{33}$$

As noted above, k_S is a parameter related to energy straggling, which can be calculated. The energy loss dE/dx is also calculable. However, the other two quantities contributing to σ_x, Doppler broadening ($\sigma_D/(dE/dx)$) and ion beam energy spread ($\sigma_b/(dE/dx)$), are in general not easily calculable, and their sum in quadrature, σ_{x0}^2, must treated as a free parameter. The value used in the fits below is the one which gives approximately the best overall fit for all the data sets.

Additionally, Eqs. (31-32) assume that the point $x_0 = 0$ corresponds to an initial ion beam energy E_0 precisely equal to the resonance energy E_r. In order to obtain good fits to the data, it was necessary to relax this assumption, and allow for a small systematic shift, ΔE, between E_0 and E_r at $x_0 = 0$. This was done by replacing x_0 with $(x_0 - \delta)$ everywhere in Eqs. (31-32), and allowing δ to be a free parameter. The relative systematic energy shift is then given by

$$\Delta E/E_0 = (\delta/E_0)(dE/dx) . \tag{34}$$

4.0 Results of Fits

Several data sets taken from Ref. 1 were fit as described above to extract values for the atomic density parameters. The data sets are defined in Table 1, and the fit results are given in Table 2. Also included in Table 2 are the calculated values for the mean "surface" density

$$\rho_S = c_1/\Lambda_1 \tag{35}$$

and the mean "equivalent-bulk" density

$$\rho_B = c_2/\Lambda_2 + c_3/\Lambda_3 . \tag{36}$$

The total effective surface density is $\rho_T = \rho_S + \rho_B$.

All calculations have used the formulas in Ref. 6, which give dE/dx = 0.339 keV/Å, and k_S = 0.310 keV^2/Å. From Ref. 1, the resonance width is taken as Γ = 1.8 keV, and the resonance energy is E_0 = 6385 keV. The best overall fit to the data sets is given using σ_{x0} = 12.5 Å (equivalent to an rms energy spread of 4.2 keV). Additional derived quantities are $k_S/(dE/dx)^2$ = 2.69 Å, and Γ_x = 5.3 Å

For data sets 2 and 4, the range of the data is not sufficient to obtain parameters for three exponentials. Hence, we have set Λ_2 = 0 and c_3 = 0.

Table 1: Description of data sets.

Data set number	Description	Figure number in Ref. 1	Data range (Å)
1	Silvex electroplated copper, cleaned	Fig. 7, 20	-60 to 4100
2	Silvex electroplated copper, not cleaned	Fig. 20	-60 to 880
3	Hitachi Class 1 OFHC copper, cleaned	Fig. 21, 10	-120 to 4070
4	Hitachi Class 1 OFHC copper, not cleaned	Fig. 21	-120 to 175

Table 2: Results of fits of effective density distributions to Eq. (8).

Data set #	c_1	c_2	c_3	$1/\Lambda_1$	$1/\Lambda_2$	$1/\Lambda_3$	$\Delta E/E_0$	ρ_S	ρ_B	ρ_T
Units	10^{22}/ cm^3	10^{22}/ cm^3	10^{22}/ cm^3	Å	Å	Å	%	10^{16}/ cm^2	10^{16}/ cm^2	10^{16}/ cm^2
1	11.70	.451	.0216	20.1	210.5	32718	-.196	2.35	8.01	10.4
2	6.28	.0958	0	79.31	------	-------	-.079	4.98	-----	-----
3	7.33	1.94	.073	23.3	80.1	1843	-.24	1.70	2.90	4.6
4	8.5	.667	0	43.5	------	-------	-.24	3.69	-----	-----

Figures 1 to 4 display the data and fits to Eqs. (31-32), on log-linear plots. As these figures show, the fit using up to three exponentials provides a good characterization of the data.

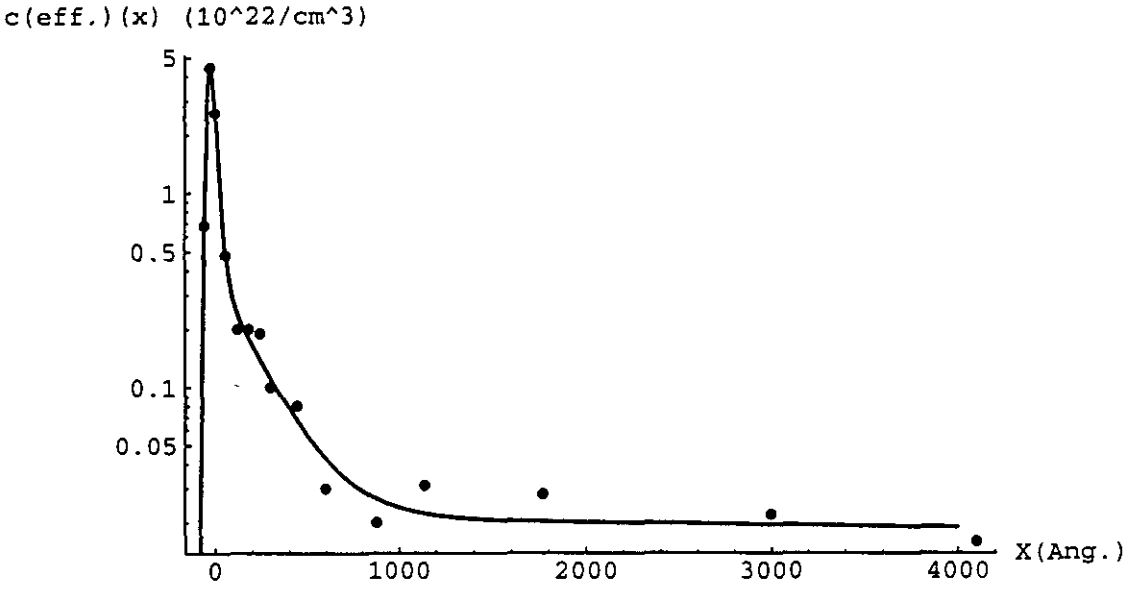

Fig. 1: "Effective" density vs. depth: data and best fit, for data set 1.

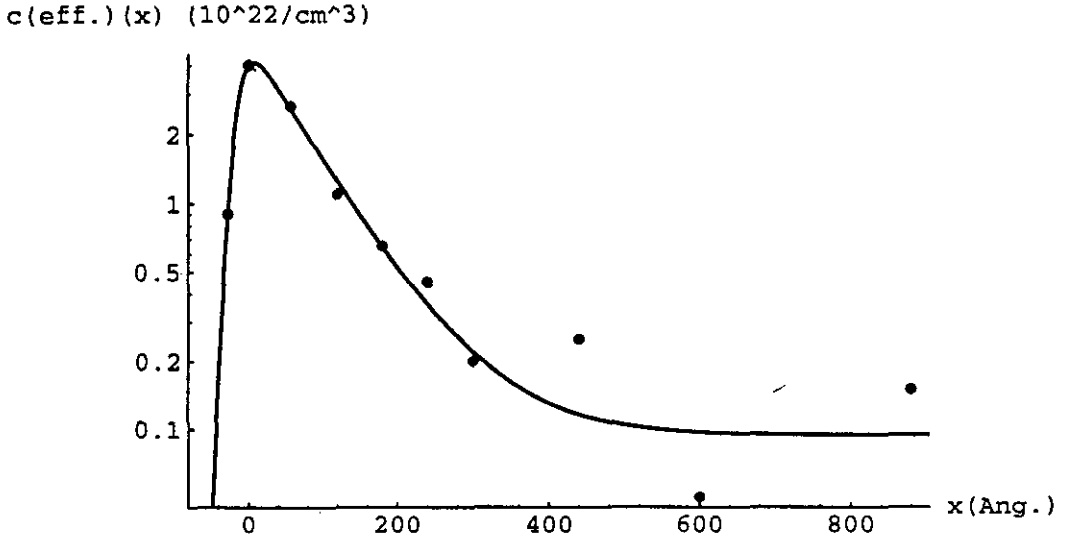

Fig. 2: "Effective" density vs. depth: data and best fit, for data set 2.

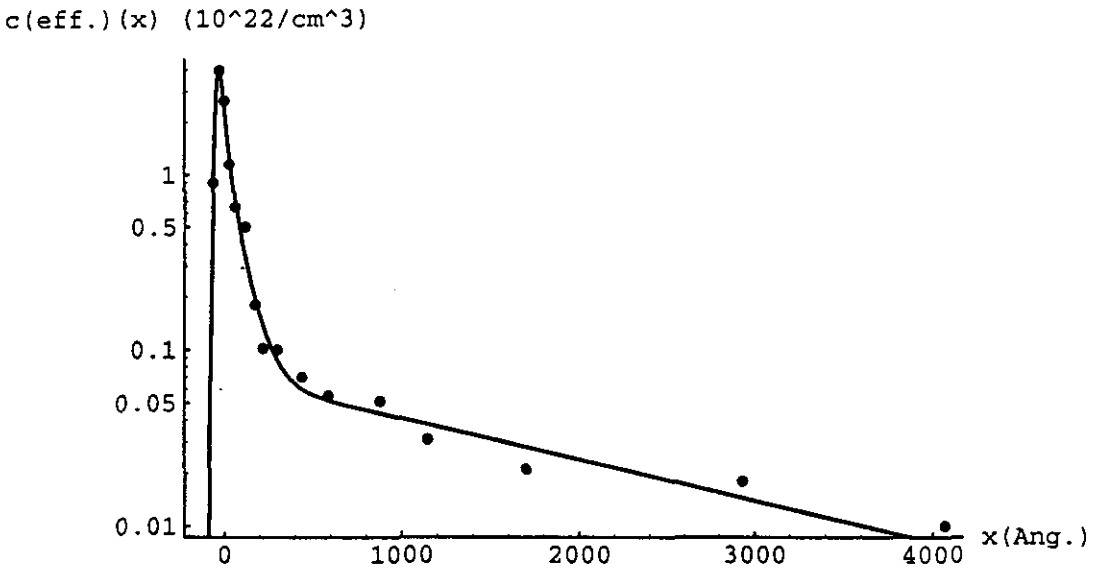

Fig. 3: "Effective" density vs. depth: data and best fit, for data set 3.

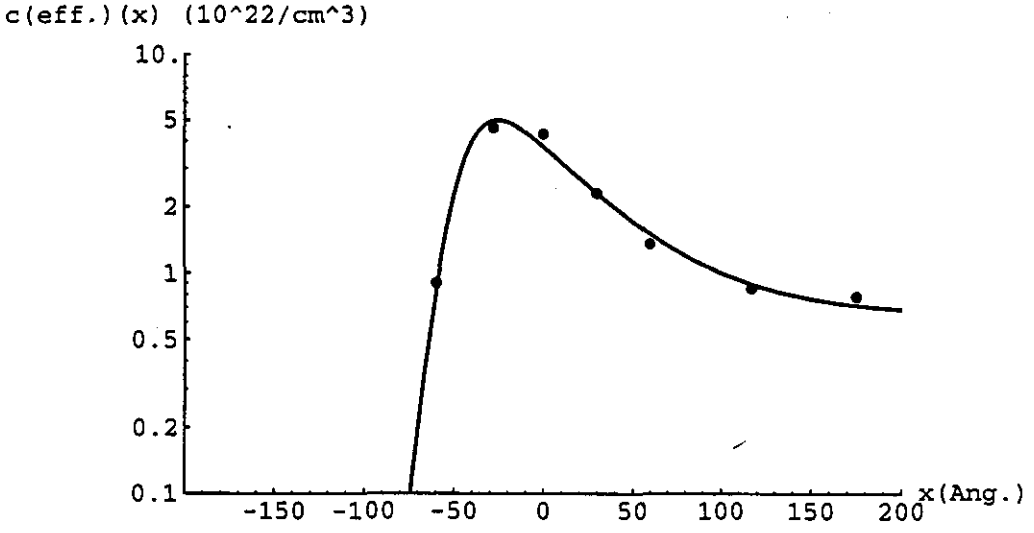

Fig. 4: "Effective" density vs. depth: data and best fit, for data set 4.

Figures 5 and 6 compare the unfolded density distributions ($c_A(x)$, from Eq. 8) for the four data sets, in linear and log plots. It is clear that data sets 2 and 4 , the "uncleaned" samples, have much larger densities at large x, *i.e.*, larger "bulk" densities, than the "cleaned" samples. They also have larger "surface" densities (as table 2 shows). However, for the Silvex electroplated copper samples, the distribution at the surface is larger for the "cleaned" sample than for the "uncleaned" one. The cleaning process appears to drive gas from the bulk to the surface, as well as removing it, but it sometimes results in a higher local gas density near the surface than in the "uncleaned" state.

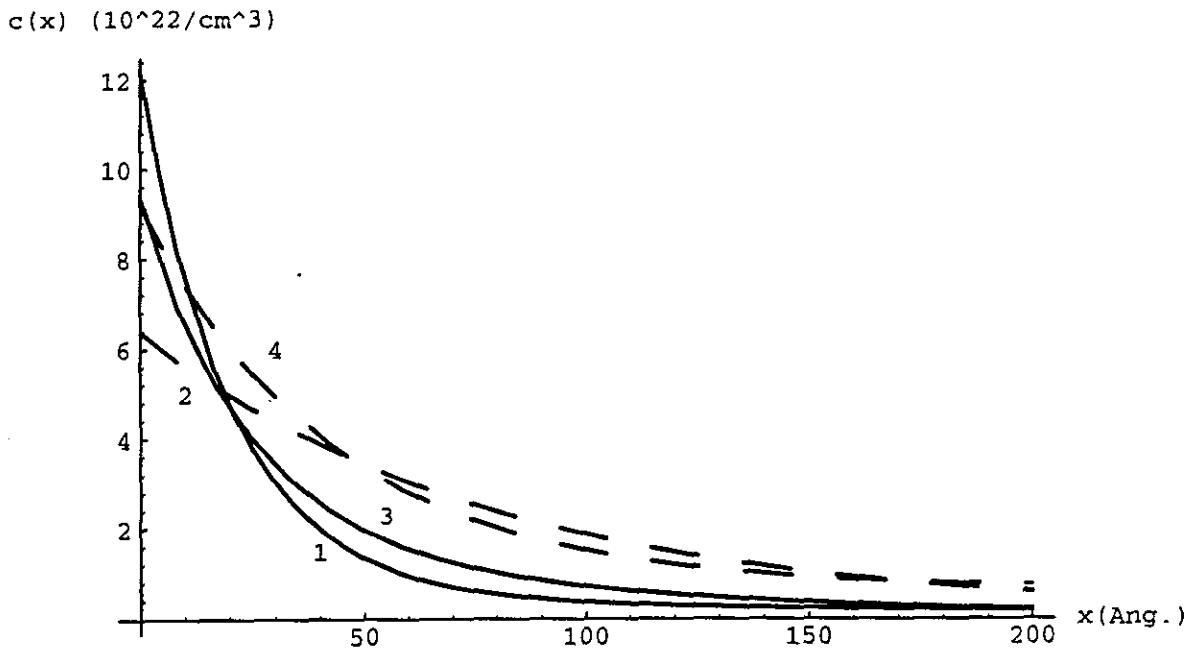

Fig. 5: Unfolded density distributions, using fitted parameters, linear plot; curves labeled by data set number. Solid lines: cleaned data; dashed lines: uncleaned data.

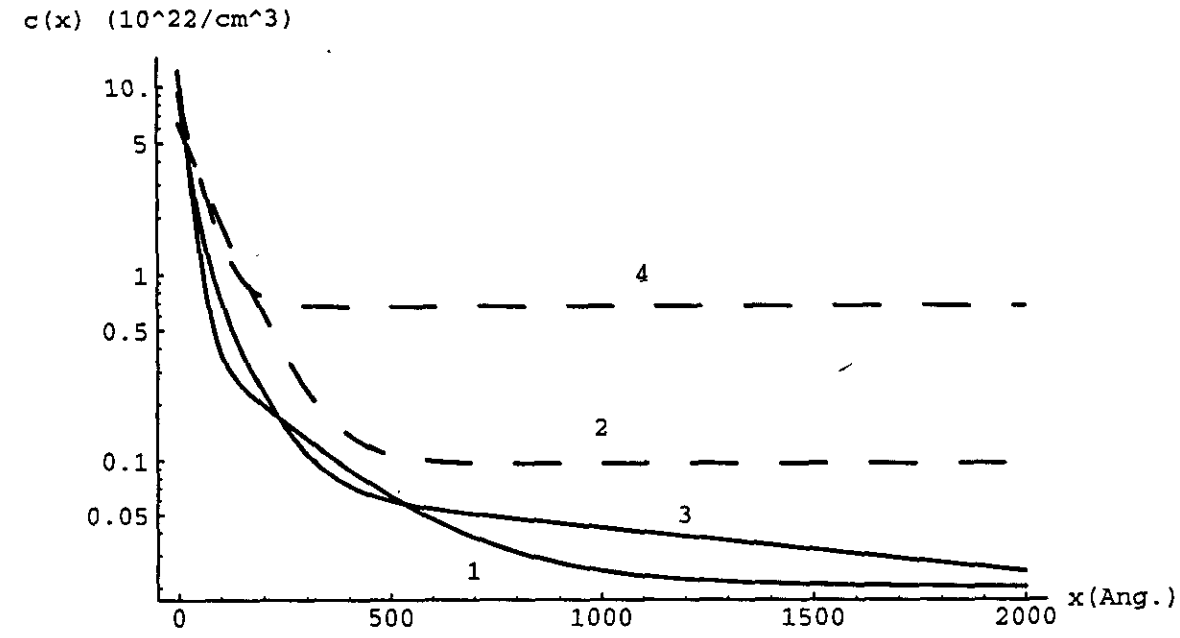

Fig. 6: Unfolded density distributions, using fitted parameters, log-linear plot; curves labeled by data set number Solid lines: cleaned data; dashed lines: uncleaned data.

5.0 Derivation of Diffusion Model Parameters from Fits to Experimental Photodesorption Coefficients, Based on Atomic Hydrogen Density Distributions

The density distributions obtained in section 3 may be used, together with Eqs. (9) to (11), to predict the photodesorption coefficient in the diffusion model. These predictions may in turn be compared with experimental photodesorption coefficient data.

This has been done for two sets of photodesorption data: one set consists of data corresponding to photodesorption in cleaned Silvex electrodeposited copper beam tubes, and another set corresponds to data for photodesorption in cleaned Hitachi copper beam tubes. The sources of the data in each case is given in Table 3.

Table 3: Sources of photodesorption data sets.

Photodesorption data set	Reference
Silvex electrodeposited copper	BINP/SSCL measurements: data sets 0009[8], 0026[9]; BNL/SSCL measurements: data sets 0017[10], 0024[11]
Hitachi copper	BNL/SSCL measurements: data set 0025[12]

For the Silvex case, the photodesorption data have been fitted to Eq. (10), using density parameters from data sets 1 and 2 of the nuclear reaction results, as given in Table 2.

For the Hitachi case, the fits have used density parameters from data sets 3 and 4 of the nuclear reaction results, as given in Table 2. In each case, the parameters D and κ in Eq. (10) have been treated as the only free parameters in the fit. The results for D and κ are given in Table 4. Also shown in Table 4 is a parameter χ^2, which characterizes the goodness of the fit. The fits to the photodesorption data are displayed in Figs. 7-10. In these figures, we plot $\mathrm{Log}_{10}\,\eta$ vs. $\mathrm{Log}_{10}\,\xi$, where $\xi = \dot{\gamma}t/\Gamma_0$, and we have used $\dot{\gamma} = 10^{14}$ photons/cm^2/sec, d=3.3 cm, and $\Gamma_0 = 10^{16}/(\pi d)$ photons/cm^2 (see Ref. 2).

Table 4: Results of fits of photodesorption data sets to diffusion model equations, based on measured concentration densities.

Photodesorption data set	Nuclear reaction data set	κ (10^{-24} cm^3)	D (10^{-18} cm^2/sec)	χ^2
Silvex electrodeposited copper	1: Silvex electrodeposited copper, cleaned	3.74	1.96	6.06
Silvex electrodeposited copper	2: Silvex electrodeposited copper, uncleaned	7.01	9.18	2.56
Hitachi copper	3: Hitachi copper, cleaned	.628	.804	.774
Hitachi copper	4: Hitachi copper, uncleaned	.581	1.18	.217

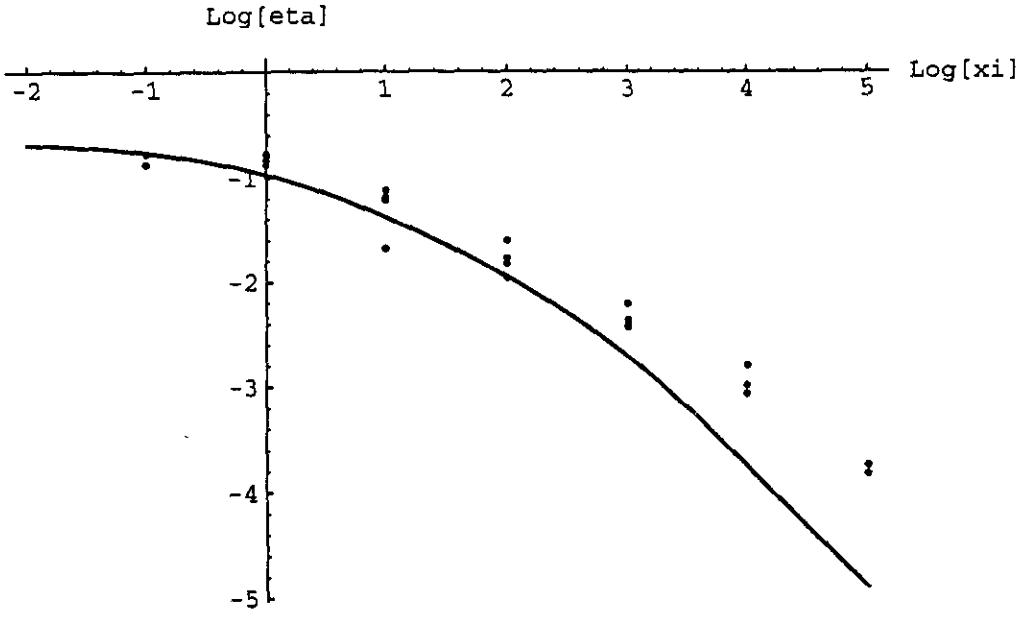

Fig. 7: Fit to Silvex electrodeposited copper photodesorption data, with cleaned Silvex electrodeposited copper density parameters.

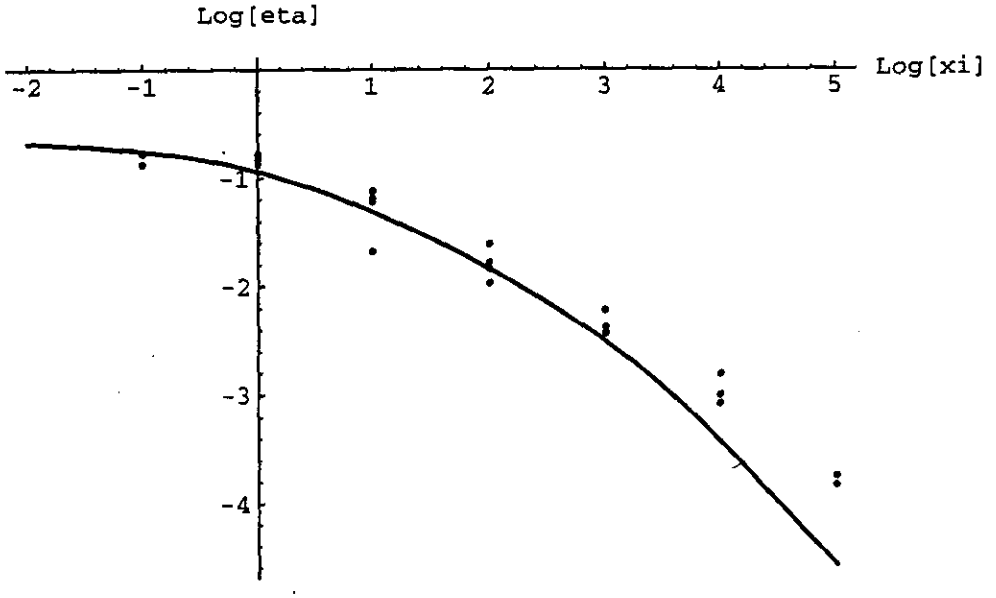

Fig. 8: Fit to Silvex electrodeposited copper photodesorption data, with uncleaned Silvex electrodeposited copper density parameters.

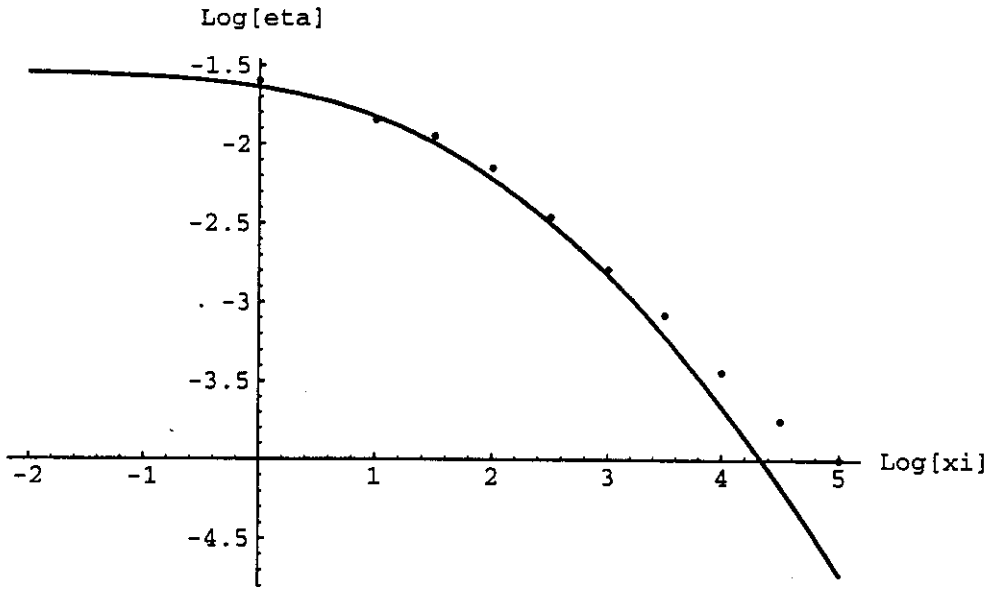

Fig. 9: Fit to Hitachi copper photodesorption data, with cleaned Hitachi copper density parameters.

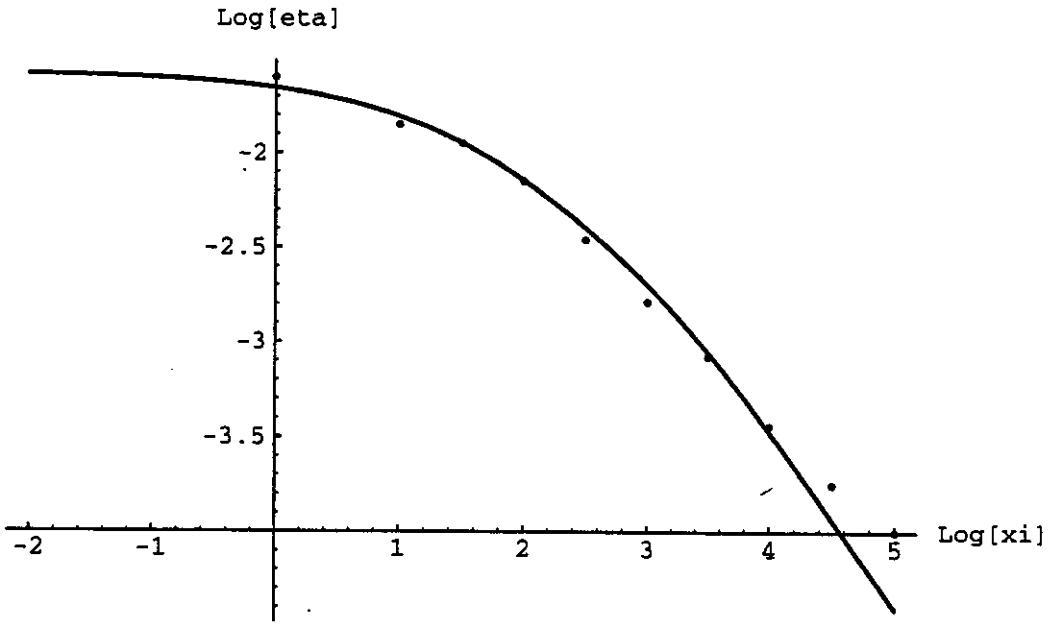

Fig. 10: Fit to Hitachi copper photodesorption data, with uncleaned Hitachi copper density parameters.

The photodesorption data at low fluxes can be fit well by any of the NRA sample hydrogen densities. However, the fits are systematically low at high fluxes. This systematic underestimate is less for the densities corresponding to the "uncleaned" samples than for the "cleaned" samples. This is due to the higher "bulk" or interior density values in the "uncleaned" samples, relative to the "surface" density. Adequate fits to the photodesorption data at high fluxes would appear to require density distributions which have an even higher ratio of "bulk" to "surface" densities than the "uncleaned" samples measured by the NRA technique.

The fits indicate a systematically smaller value for the parameter κ for the Hitachi copper samples than for the electrodeposited copper ones. From Eq. (1), this would imply a larger value of λ, the mean depth of effective photon interaction, in the electrodeposited copper surface than in the Hitachi copper. Such a result could be due to a more diffuse or "rough" character (at the micron level) of the surface of the electrodeposited sample, compared to the surface of the high purity Hitachi copper.

References

1. M. W. Ruckman, M. Strongin, W. A. Langford "Nuclear Reaction Analysis of Hydrogen in SSC Beam Pipe Materials," SSCL-N-836, November 1993.
2. G. Dugan, "Interpretation of Photodesorption Data in a Diffusion Model and Application to Candidate SSC beam Tube Surfaces," SSCL-610, January 1993.
3. M. Abramowitz, I. Stegun, "Handbook of Mathematical Functions," p. 302, Dover (New York), 1970.
4. Ibid., pg. 299.
5. I. S. Gradshteyn, I. M. Ryzhiz, *Table of Integrals, Series and Products,* p. 481, Academic Press (New York), 1980.
6. J. F. Ziegler, J. P. Biersack, and U. Littmark, *The Stopping and Range of Ions in Solids*, vol. **1**, Pergamon Press (New York), 1985.
7. W. A. Lanford, "Analysis for hydrogen by nuclear reaction and energy recoil detection," *Nucl. Inst. and Meth.* **B66** (1992), p. 65-82.
8. I. Maslennikov, "SSCL Photodesorption Experiments at BINP, Russia and BNL," in *Vugraph Presentations from the Proton Collider Vacuum Technical Meeting* (Nov. 1992).
9. V. Anashin *et al.*, "Summary of Recent Photodesorption Experiments at VEPP2M," SSCL-N-823, June 1993.
10. C. L. Foerster, "Photodesorption Measurements of Warm Beam Tube Samples," in *Vugraph Presentations from the Second Proton Collider Vacuum Technical Meeting,* (May 1993), (BNL Run #1).
11. I. Maslennikov *et al.*, "Photodesorption Experiments on SSC Collider Beam Tube Configurations," in *Proceeding of the 1993 Particle Accelerator Conference*, Washington D.C. (1993), pg. 3876.
12. C. L. Foerster, "Photodesorption Measurements of Warm Beam Tube Samples," in *Vugraph Presentations from the Second Proton Collider Vacuum Technical Meeting,* (May 1993), (BNL Run #2).

TIP prepared Figures

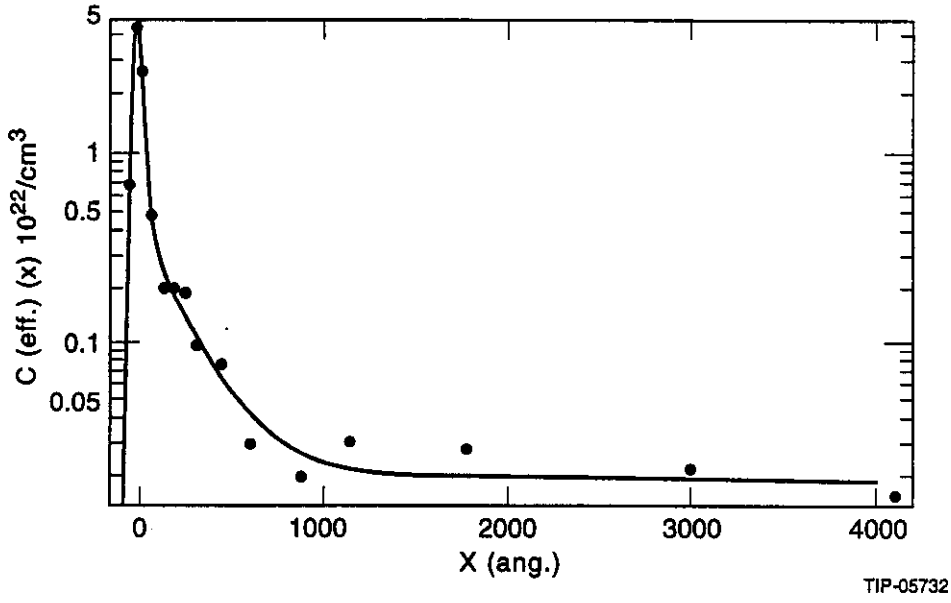

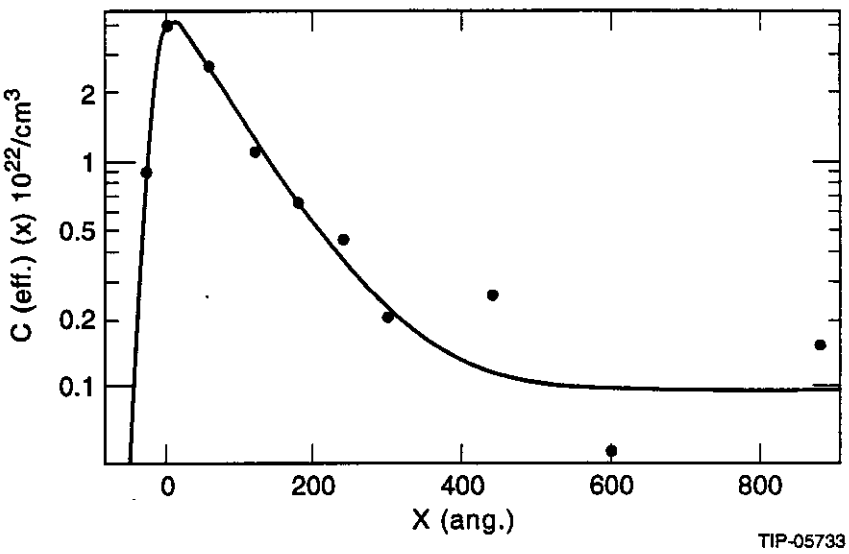
C (eff.) (x) 10^{22}/cm^3
2
1
0.5
0.2
0.1
0
200
400
600
800
X (ang.)
TIP-05733

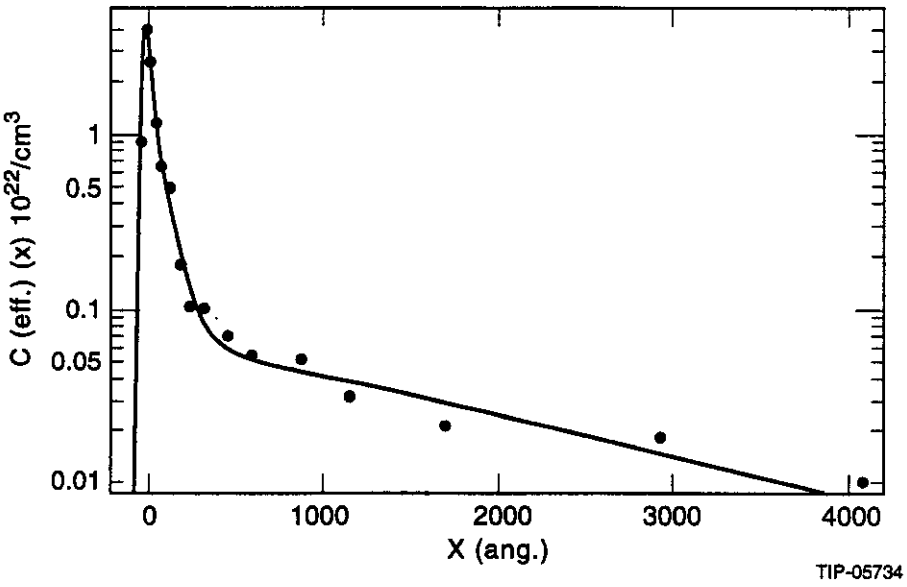
C (eff.) (x) 10^{22}/cm^3
1
0.5
0.1
0.05
0.01
0
1000
2000
3000
4000
X (ang.)
TIP-05734

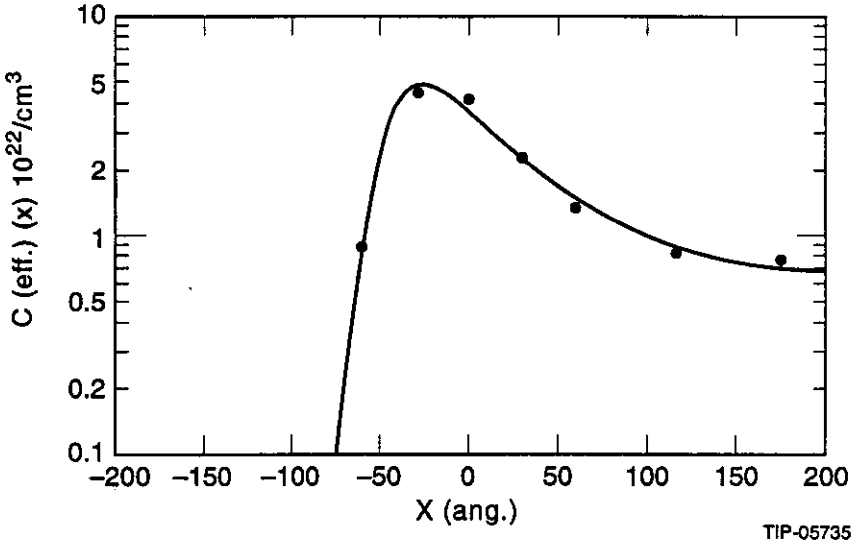
10
5
2
1
0.5
0.2
0.1
C (eff.) (x) 10^{22}/cm^3
−200
−150
−100
−50
0
50
100
150
200
X (ang.)
TIP-05735

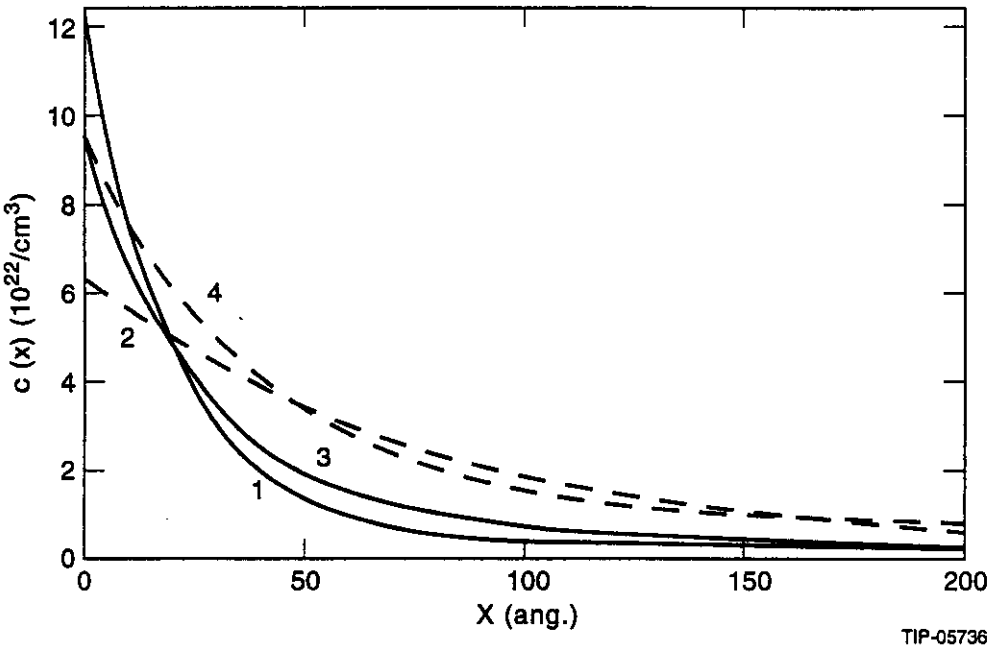
12
10
8
6
4
2
0
c (x) (10^{22}/cm^3)
0
50
100
150
200
X (ang.)
1
2
3
4
TIP-05736

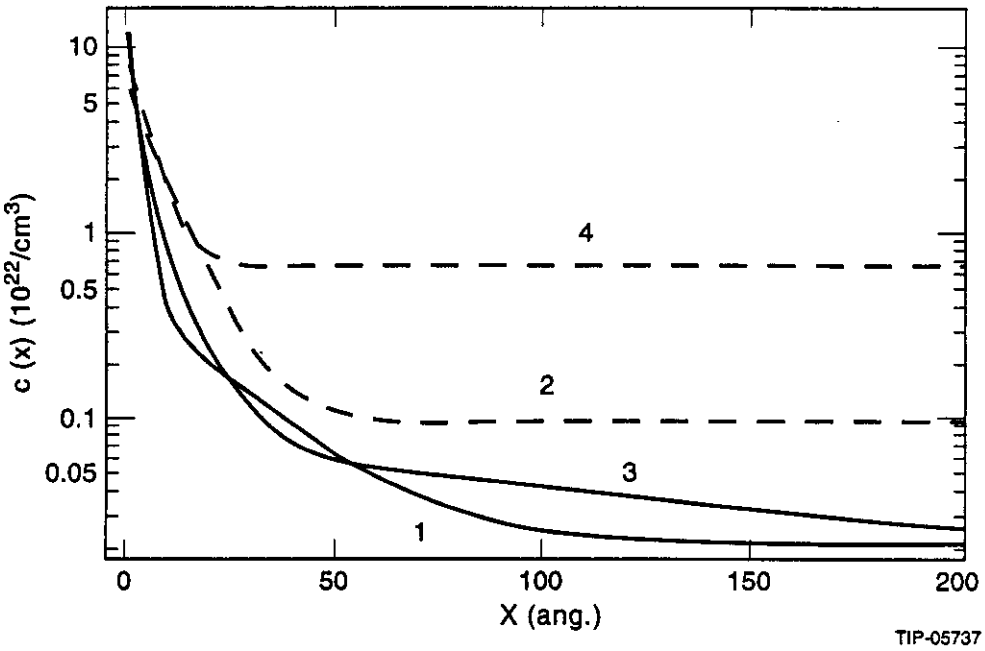
10
5
1
0.5
0.1
0.05
c (x) (10^{22}/cm^3)
4
2
3
1
0
50
100
150
200
X (ang.)
TIP-05737

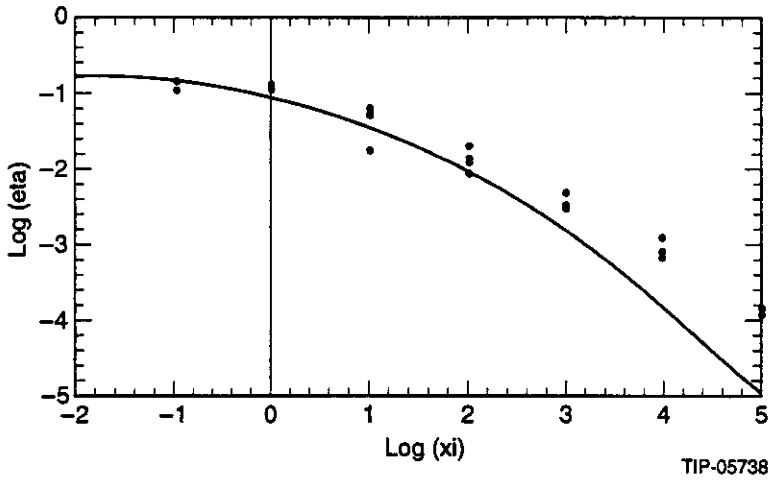
0
−1
−2
−3
−4
−5
Log (eta)
−2
−1
0
1
2
3
4
5
Log (xi)
TIP-05738

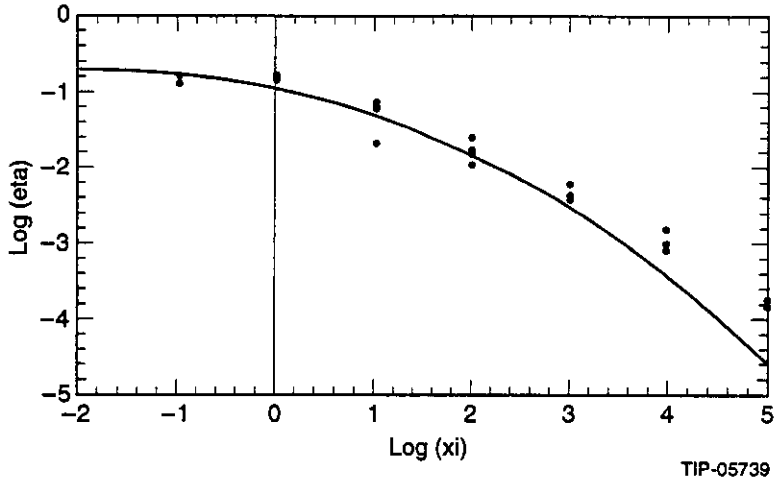
0
−1
−2
−3
−4
−5
Log (eta)
−2
−1
0
1
2
3
4
5
Log (xi)
TIP-05739

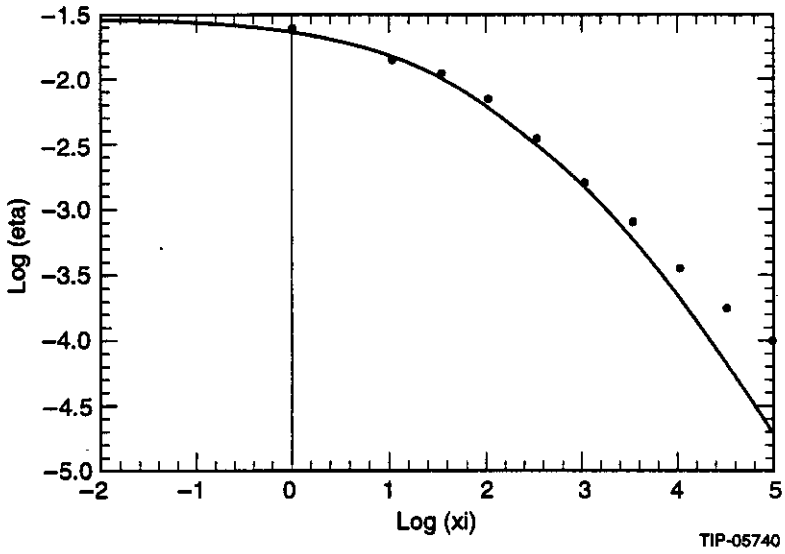
−1.5
−2.0
−2.5
−3.0
−3.5
−4.0
−4.5
−5.0
Log (eta)
−2
−1
0
1
2
3
4
5
Log (xi)
TIP-05740

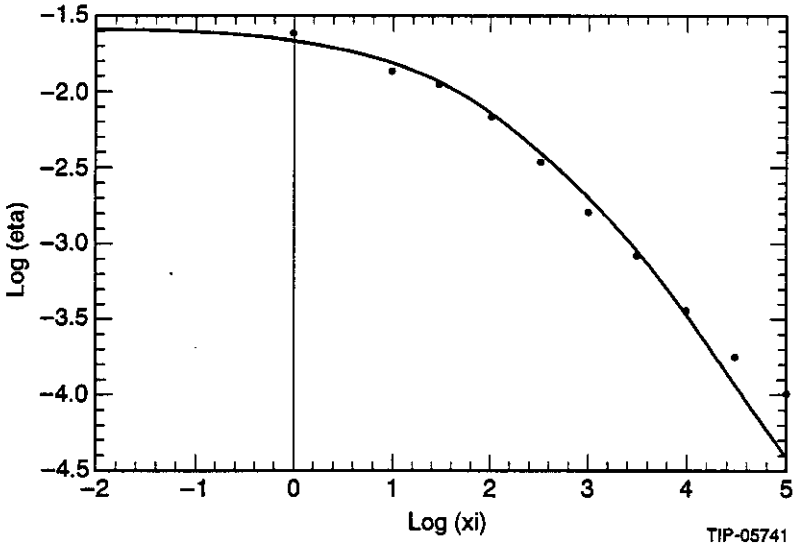
−1.5
−2.0
−2.5
−3.0
−3.5
−4.0
−4.5
Log (eta)
−2
−1
0
1
2
3
4
5
Log (xi)
TIP-05741